astronomy

MDPI

Article

Chandra Observations of the X-Ray Binary Population in the Field of the Dwarf Galaxy IC 10

Sayantan Bhattacharya [1,*,†,‡], Silas G. T. Laycock [1,†], Breanna A. Binder [2,†] and Dimitris M. Christodoulou [1,*,†,§]

[1] Lowell Center for Space Science and Technology, University of Massachusetts Lowell, Lowell, MA 01854, USA; silas_laycock@uml.edu
[2] Department of Physics and Astronomy, California State Polytechnic University, Pomona, CA 91768, USA; babinder@cpp.edu
* Correspondence: sayantan.bhattacharya@tifr.res.in (S.B.); dimitris_christodoulou@uml.edu (D.M.C.)
† The authors contributed equally to this work.
‡ Current address: Tata Institute of Fundamental Research, Homi Bhabha Road, Colaba, Mumbai 400005, India.
§ Current address: Department of Mathematical Sciences, DePaul University, Chicago, IL 60614, USA.

Abstract

IC 10 is a dwarf galaxy in Cassiopeia, located at a distance of 660 kpc, and hosts a young stellar population, a large number of Wolf–Rayet stars, and a large number of massive stars in general. Utilizing a series of 11 *Chandra* observations (spanning 2003–2021, with a total exposure of 235.1 ks), 375 point sources of X-ray emission were detected. Similar studies have been conducted earlier in the central region of IC 10. Here, we consider all regions covered by *Chandra-ACIS*. By comparing our catalog of X-ray sources with a published optical catalog, we found that 146 sources have optical counterparts. We also created a list of 60 blue supergiant (SG) candidates with X-ray binary (XRB) companions by using an optical color–magnitude selection criterion to isolate the blue SGs. Blue SG-XRBs form a major class of progenitors of double-degenerate binaries. Hence, their numbers are an important factor in modeling the rate of gravitational-wave sources. Identifying the nature of individual sources is necessary as it paves the way toward a comprehensive census of XRBs in IC 10, thus enabling meaningful comparisons with other Local Group galaxies exhibiting starbursts, such as the Magellanic Clouds.

Keywords: X-ray astronomy; X-ray binaries; star formation; blue supergiant stars; catalogs; galaxy IC 10

Received: 13 September 2025
Revised: 11 November 2025
Accepted: 9 December 2025
Published: 13 December 2025

Citation: Bhattacharya, S.; Laycock, S.G.T.; Binder, B.A.; Christodoulou, D.M. *Chandra* Observations of the X-Ray Binary Population in the Field of the Dwarf Galaxy IC 10. *Astronomy* **2025**, *4*, 26. https://doi.org/10.3390/astronomy4040026

1. Introduction

IC 10 is a young starburst galaxy in the constellation Cassiopeia. This irregular galaxy is a part of the Local Group [1,2] at a distance of 660 kpc from our galaxy (the measurements range from 660 [3] to 817 [4] kpc). It is an excellent laboratory for studying the high-mass X-ray binaries (HMXBs) containing the most massive young stars. This galaxy is also a subject of multiple observations due to its highly dense Wolf–Rayet stellar population. The high number of Wolf–Rayet (WR) stars discovered by Massey et al. [5] and Massey and Armandroff [6] was the primary indicator of IC 10's starburst nature. These investigations were spurred on by the discovery of 144 H II regions by Hodge and Lee [7]. The brightest H II region in IC 10 is on par with the brightest such region observed in the SMC [8]. The surface density of WR stars throughout IC 10 is similar to that of the most active OB associations in M33 [9]. Wilcots and Miller [10] suggested that IC 10 is undergoing a

starburst, probably triggered by gas infalling from an extended cloud that counter-rotates relative to the galaxy's proper motion.

The Local Group, which includes about 55 galaxies in a volume of diameter 3 Mpc, is the term used to identify our own neighborhood in the universe. IC 10 is one of the irregular dwarf galaxies that resides in the Local Group, although it is relatively far from the two most massive galaxies, our galaxy and M31. The galaxy has been described as a blue compact dwarf (BCD) because of its surface brightness after taking into account foreground reddening [11]. However, it is situated at a very low galactic latitude ($\ell = 119.0°$, $b = -3.3°$); thus, its line of sight is heavily affected by foreground reddening, which hampers optical observations. IC 10 consists of the main body and several distinct star-forming regions. Several H I holes are found throughout the galaxy, which are most probably the cumulative effect of powerful stellar winds [12]. The overall structure indicates recent widespread star formation activity.

IC 10 presents a suitable environment for studying multiple physical properties due to its similarities with the LMC and the SMC. The SMC and IC 10 have a lot in common: they are both gas-rich irregular dwarfs believed to have experienced tidal disruption recently, which sparked intense star formation. Two significant characteristics, however, set IC 10 apart and make it a new type of laboratory for stellar astrophysics: (a) The duration of its starburst is only 6 Myr, whereas the ages of the populations discovered in the SMC range between 40 and 200 Myr, where the HMXBs are found in the 40–70 Myr subpopulation [13]. (b) The metallicity of IC 10 ($Z = Z_{\odot}/5$) is midway between those of the SMC and the Milky Way.

Comprehensive censuses of X-ray binary populations in Local Group galaxies offer an effective approach to identifying the fundamental properties of star formation and evolution, such as starburst age/duration and the impact of the host's metallicity. The Magellanic Clouds have historically played this role, but new independent testbeds (like IC 10 and NGC 300) must be utilized in order to properly understand secular variances between galaxies. For instance, a detailed analysis of the data set reported on here has shown that a recent (3–8 Myr) star-forming event with a rate of $\sim 0.5\, M_{\odot}\ \mathrm{yr}^{-1}$ is needed to explain the current XRB population of IC 10 [14].

The Local Group's maximum surface density of WR stars is found in IC 10, yet the ratio of WC/WN spectral classes differs from that predicted by stellar evolution models for a galaxy with such low metallicity. Thus, the WC/WN ratio in IC 10 is certainly peculiar, notwithstanding the recent discovery of three new WN stars, which reduce the ratio from 1.3 to 1.0. So, IC 10 is still regarded as an anomaly given the WC/WN ratio of ∼0.2 for the LMC and ∼0.1 for the SMC. However, this marked difference also suggests that the starburst observed in IC 10 is quite recent.

IC 10 is also a functional testbed for studying HMXB populations. In young starburst galaxies (<10 Myr), the X-ray populations are expected to consist of massive stars and neutron star or black hole (NS or BH) binaries. IC 10 is the nearest among such galaxies. For these reasons, we used archival and new *Chandra* X-ray data from multiple epochs to monitor the transient X-ray population of IC 10.

This article is arranged in the following way: The observations and data reductions are described in Section 2. The main results are presented and analyzed in Sections 3–6. A discussion of the underlying populations and a summary along with conclusions are included in Sections 7 and 8, respectively.

2. Observations: New and Archival

IC 10 has been the target of multiple X-ray observations (11 *Chandra*, 2 *XMM-Newton*, 1 *NuSTAR*, and many *Swift* snapshots). *Chandra* and *Swift*, in particular, have repeatedly

observed the galaxy to monitor its numerous X-ray sources, including the very bright WR+BH system IC 10 X-1. Wang et al. [15] first analyzed the combined spectra from single pointings of *XMM* and *Chandra*. They discovered a population of X-ray point sources (28 from *Chandra* and 73 from *XMM-Newton*) above the background. The sources were mostly concentrated within the optical outline of IC 10. The combined X-ray spectrum also showed physical properties and derived parameters characteristic of HMXBs.

Laycock et al. [16] performed a complete census of all X-ray sources in the central region of IC 10 using *Chandra ACIS S3* data from 10 observations spanning 2003–2010 and found 110 X-ray point sources. Our work is a follow-up of the effort made by Laycock et al. [16] and extends the existing catalog of XRBs using all available *Chandra* observations and all CCDs that were turned on during observations. Since the full field of view of *Chandra* was used, our catalog includes all sources detected in the IC 10 field. As a result, not all detected X-ray sources may be physically associated with the galaxy. Some sources are bound to be foreground stars or background AGN.

IC 10 has been observed repeatedly by *Chandra* since 2003. The X-ray observations include a monitoring series of seven 15 ks exposures that were key to identifying 21 sources that were variable to a 3σ level. A pair of deep observations in 2006 that served as a reference data set also exists. The first-ever 2003 data set [15] (Obsid: 03953, ACIS-S in subarray mode) and the latest 2021 data set (Obsid: 26188) were also included in our data set. The new observations provided an expanded temporal baseline for X-ray source monitoring. The complete list of *Chandra* observations used to create the final X-ray source catalog is summarized in Table 1.

Table 1. *Chandra* X-ray observation log.

Observatory	Instrument	Observation Date (MJD)	Observation ID (Obsid)	Exposure Time (ks)
CXO	ACIS	52,710.7	03953	28.9
CXO	ACIS	54,041.8	07082	40.1
CXO	ACIS	54,044.2	08458	40.5
CXO	ACIS	55,140.7	11080	14.6
CXO	ACIS	55,190.2	11081	8.1
CXO	ACIS	55,238.5	11082	14.7
CXO	ACIS	55,290.6	11083	14.7
CXO	ACIS	55,337.8	11084	14.2
CXO	ACIS	55,397.5	11085	14.5
CXO	ACIS	55,444.6	11086	14.7
CXO	ACIS	59,586.3	26188	30.1

2.1. Data Reductions

The reduction and analysis of *Chandra* data were conducted by exclusively using CIAO, the dedicated software suite developed by the Chandra X-ray Center. CIAO (version 4.17) can be installed via the Anaconda-based Python environment (version 3.11) or the `ciao-install` script, available at https://cxc.cfa.harvard.edu/ciao/download/ (accessed on 10 September 2025). Data were downloaded directly from the *Chandra* archives using the command-line tool `download_chandra_obsid`, which supports queries using source names or coordinates with a specified search radius. Once the raw data were obtained, they were reprocessed using the `chandra_repro` command, which generates a new 'repro' directory containing cleaned event files. These event files were further corrected to the solar system barycenter using the `axbary` tool.

Prior to source detection, exposure-corrected images in different energy bands were generated using the `fluximage` script, which also creates exposure and PSF maps. The

main source detection for the current project relies on `wavedetect`. This tool was applied to images in broad (0.3–8 keV), soft (0.3–1.5 keV), medium (1.5–3 keV), and hard (3–8 keV) bands using wavelet scales of 1, 2, 4, 8, and 16 pixels and a significance threshold of 10^{-6}.

2.2. X-Ray Images and Source Detections

The main focus of this work was to create a comprehensive catalog of X-ray sources using all available observations (listed by Obsid in Table 1). Merged images for visual inspection were also created with Gaussian smoothing in all energy bands.

The source detection algorithm `wavedetect` was first run on each Obsid and energy band. This created a source list with many parameters, including position and position uncertainties, counts, PSF shape, detection significance, etc. Each source list was then boresight-corrected using the coordinates of the brightest source (IC 10 X-1). These lists were then used for further cross-matching and the creation of the final catalog, as described below.

The *wavedetect* source lists were cross-matched within the energy bands first to create a single source list for each observation. Then, the source lists of all the observations were combined to create the final X-ray source catalog. Cross-matching was conducted using the *classifytable* tool in the command-line-based relational database software package *Starbase*.

The tool *classifytable* groups together sources that lie within a distance of 5″, which are then further filtered by the r_{95} error radius of each source. While matching the lists, the `wavedetect`-provided error radius was not used to look for proximity. Instead, the 95% uncertainty radius r_{95} was calculated using the Hong et al. [17] prescription. Also, when considering which instance of a source (detected in multiple observations) to include in the final catalog, the one with the minimum value of r_{95} was chosen.

In the last step, our latest catalog, the previous version from Laycock et al. [16], the Chandra source catalog (CSC 2.3), and the XMM source catalog (4XMM DR13) were all combined to generate the final unique source catalog that contains one entry for each X-ray source with its position and position uncertainty radius r_{95} (provided as supplementary material in Ref. [18]).

3. Long-Term Lightcurves and Variability

Understanding the variability in these X-ray sources was a major motivation for this campaign. We used CIAO's `srcflux` tool to extract the count rates R for each source in the X-ray catalog. This enabled us to create a long-term lightcurve for all X-ray sources (provided as supplementary material in Ref. [18]).

The variability in a source can be quantified by the flux variability ratio ($F_{\max}/F_{\min}$) and the variability count rate range ($\Delta R = R_{\max} - R_{\min}$). The count rates in the broad band were converted to relative variabilities ($\sigma_{\rm var}$) using the standard prescription

$$\sigma_{\rm var} \;=\; \Delta R / \sqrt{error[(R_{\max})^2] \;+\; error[(R_{\min})^2]}\,.$$

These quantities were calculated for each individual source, and the strongly variable sources with $\sigma_{\rm var} \geq 5$ (as in Ref. [14]) are listed in Table 2. Some of these sources are discussed further in Section 7.

Table 2. Variability measurements for sources with relative values of $\sigma_{\rm var} \geq 5$.

Source #	$\mathbf{R_{max}}$	$\mathbf{R_{max}^{error}}$	$\mathbf{R_{min}}$	$\mathbf{R_{min}^{error}}$	ΔR	$\sigma_{\rm var}$	No. in FOV	No. Detected
5	0.00264	0.00030	0.00010	0.00006	0.00234	8.28	11	11
8	0.00528	0.00035	0.00179	0.00025	0.00493	8.20	11	11
12	0.00684	0.00040	0.00263	0.00044	0.00644	7.13	11	11
20 (X-1)	0.15651	0.00232	0.02079	0.00118	0.15419	52.20	11	11
23	0.00141	0.00018	0.00013	0.00007	0.00123	6.57	11	11
28	0.00265	0.00025	0.00010	0.00006	0.00240	9.96	11	11
41	0.00154	0.00019	0.00007	0.00007	0.00135	7.36	11	9
46 (X-2)	0.01014	0.00059	0.00007	0.00007	0.00955	16.98	11	8
52	0.00110	0.00016	0.00013	0.00010	0.00094	5.22	9	8
63	0.00096	0.00015	0.00007	0.00007	0.00081	5.44	10	8
112	0.00882	0.00077	0.00214	0.00022	0.00805	8.33	4	4
121	0.00484	0.00057	0.00174	0.00020	0.00427	5.13	5	5
126	0.00727	0.00070	0.00343	0.00028	0.00657	5.09	3	3
130	0.00465	0.00056	0.00131	0.00031	0.00409	5.21	5	5
136	0.00269	0.00043	0.00034	0.00009	0.00226	5.40	5	5
137	0.00296	0.00045	0.00063	0.00012	0.00251	5.03	5	5
141	0.18591	0.00354	0.06287	0.00208	0.18237	29.99	6	6
146	0.00364	0.00049	0.00050	0.00011	0.00315	6.18	6	6
220	0.00197	0.00037	0.00007	0.00007	0.00160	5.08	3	3
229	0.00278	0.00043	0.00003	0.00003	0.00235	6.31	4	4
246	0.00321	0.00048	0.00040	0.00016	0.00273	5.49	4	4
268	0.00511	0.00061	0.00128	0.00029	0.0045	5.66	3	3
299	0.00154	0.00019	0.00013	0.00010	0.00135	6.66	6	6
313	0.00358	0.00051	0.00074	0.00022	0.00307	5.09	4	4
314	0.00139	0.00018	0.00013	0.00010	0.00121	6.13	5	5
315	0.00296	0.00045	0.00015	0.00010	0.00251	6.14	5	5
329	0.01131	0.00087	0.00128	0.00021	0.01044	11.18	5	5
361	0.00639	0.00066	0.00040	0.00016	0.00573	8.86	3	3
362	0.00323	0.00047	0.00034	0.00015	0.00276	5.90	4	4
363	0.00269	0.00043	0.00040	0.00016	0.00226	5.01	3	3
364	0.00525	0.00059	0.00027	0.00014	0.00466	8.16	4	4
365	0.00606	0.00064	0.00020	0.00012	0.00542	9.02	3	3
366	0.00565	0.00062	0.00014	0.00010	0.00503	8.84	3	3
370	0.00231	0.00040	0.00007	0.00007	0.00191	5.58	2	2
371	0.00680	0.00068	0.00199	0.00037	0.00612	6.24	3	3

4. Catalog of X-Ray Binaries

A young starburst galaxy like IC 10 is expected to have a stellar population dominated by HMXBs. Motivated by earlier works, we proceeded to match the final XRB catalog with the Massey et al. [19] optical catalog of IC 10 stars. This photometric catalog has a limiting magnitude of $V = 23.8$. Using their catalog of ACIS S3 observations of 110 X-ray sources, Laycock et al. [16] found optical counterparts to 42 of these sources.

We increased the number of X-ray sources to 375 (compared to Ref. [16]), and we matched them again with the same optical catalog. *Starbase* was used to look for optical counterparts within the total radius of r_{95} plus $1''$ added in quadrature (viz. $\sqrt{(r_{95})^2 + 1^2}$) to account for systematic uncertainties. We found 146 X-ray sources with optical counterparts (a 3.5-fold increase);=, whereas the remaining 229 sources do not have counterparts down to the limiting magnitude of $V = 23.8$. The X-ray source IDs along with the properties of their optical counterparts are listed in Tables A1–A4 of Appendix A.

5. Blue Supergiant X-Ray Binaries

IC 10 is known to host many blue supergiants (BSGs) and Wolf–Rayet and massive stars in general. Hence, in the next step, we further investigated these 146 binary systems using the characteristics of their optical counterparts. An important physical parameter in this endeavor is the optical source colors and the resulting color–magnitude diagram (Figure 1). At the distance (660 kpc) and reddening ($\mu = 24$, $A_V = 3$, and E_{B-V} = 0.85–1.09) of IC 10 [20,21], the main sequence beyond spectral type B0V is not visible in ground-based telescope images, but BSGs, the most luminous stars, are certainly visible. Foreground stars are also located in the field of IC 10 because the line of sight passes through the outermost region of the Galactic Plane. Fortunately, the main sequence (defined by the galactic stars) is well separated from the BSG branch in color—magnitude space after correction due to reddening.

The limiting magnitude of the optical catalog also limits our search for HMXBs. Antoniou et al. [13] predict that the HMXB counterparts are hotter than B3 and that the peak of the distribution is around B0. Hence, we are missing ∼50% of the population. Accounting for the reddening vector in the direction of IC 10 X-2 ($V = 19.954$, $E_{B-V} = 1.09$; Table 3 shown in Ref. [20]), we used a filter of $V > 19.5$ and $B - V < 1.5$ among the 146 optical counterparts, and we found 60 BSG candidates (about 40% of the sample; Figure 1). The BSG candidates are listed in Tables A5 and A6 along with their X-ray source ID, coordinates, V magnitude, and color information.

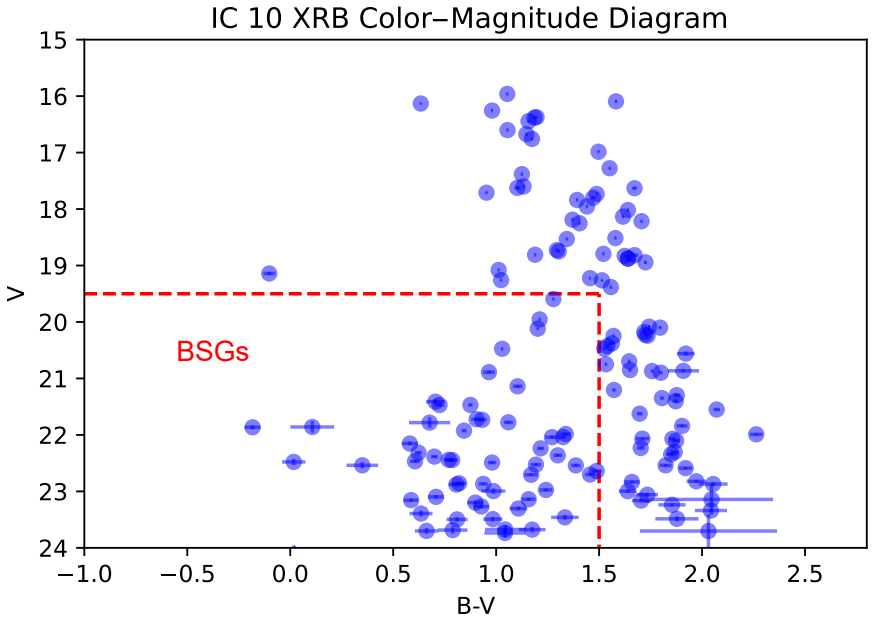

Figure 1. A color–magnitude diagram of the optical counterparts of 146 X-ray sources. The dashed box indicates the selection region for 60 BSG candidates, which are expected to have $V > 19.5$ and $B - V < 1.5$.

6. Peak-Up Test for Positional Accuracy

Studying X-ray binaries enables the identification and characterization of both the X-ray compact object and the optical stellar companion, as well as the confirmation of their association. The identification of optical counterparts is a problem often encountered in astronomy, and there are various robust methods used in the literature for this purpose [22–24].

In general, when the objects under investigation are rare and both catalogs have good positional accuracy, astronomers consider positional alignment to imply physical

association. This is a risky and unnecessary assumption given that there exists a quantitative approach, the so-called 'peak-up test' [21]. This test can be applied to *Chandra* observations of crowded fields, where there is a non-negligible chance of accidental alignment and a positional uncertainty for each X-ray source.

In the peak-up test, two catalogs are repeatedly matched with one other [21]. In each iteration, a small offset in the coordinate system is applied, and the list of matching objects is recorded. The offsets are arranged in a regular grid spacing in (RA, DEC). The spacing is kept finer than the positional accuracy of the input catalogs, and the total offset extends to several times the radius of the largest error circles.

The significance of the peak in the peak-up map (Figures 2 and 3) is tied to the local surface density of optical sources. At large artificial offsets, the number of matches converges to the expected number of random coincidences $\bar{n}$, which can be estimated by

$$\bar{n} = \rho_{\mathrm{opt}}\left(\pi r_{\mathrm{m}}^{2}\right) n_{\mathrm{x}},$$

where ρ_{opt} is the local surface density of optical sources in $(\mathrm{arcsec})^{-2}$, $r_{\mathrm{m}} = \sqrt{(r_{95})^2 + 1^2}$ is the adopted matching radius in arcsec, and n_{x} is the number of matched X-ray sources. The peak observed at zero offset represents an excess $(n_{\mathrm{x}} - \bar{n})$ above the random background and quantifies the number of true physical associations. The peak-up test characterizes by default the local density function because the height of the peak is determined by the contrast between true matches and the local random match rate.

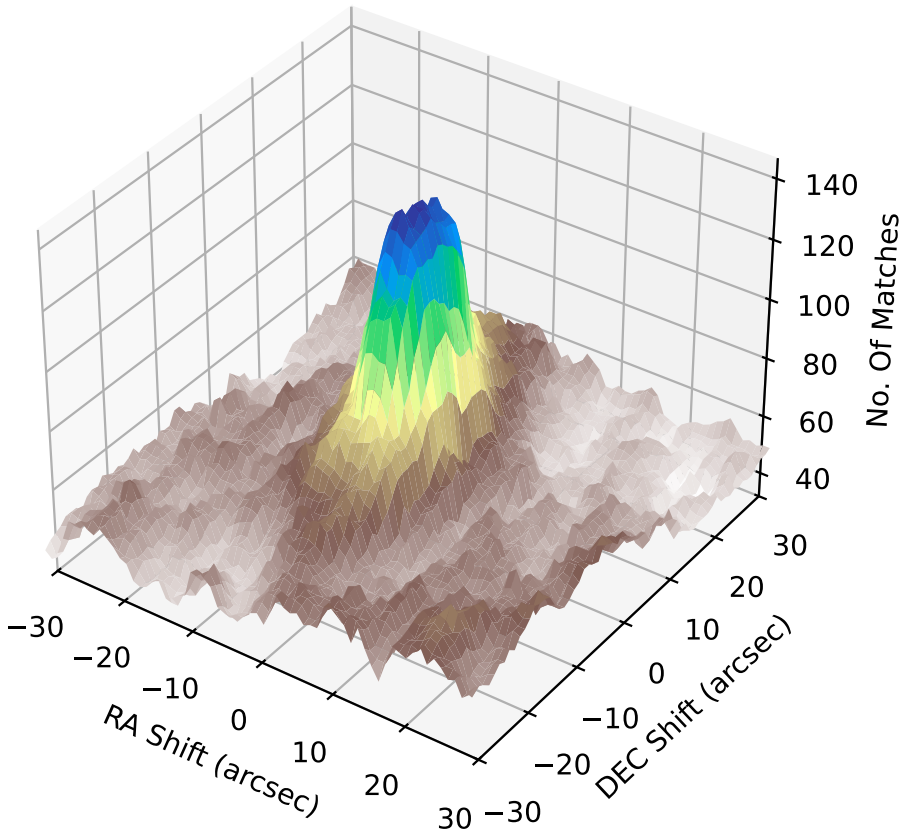

Figure 2. The peak-up test result for XRB counterparts in IC 10. The plot shows the number of matches $(n_{\mathrm{x}} - \bar{n})$ between X-ray and optical sources as a function of small coordinate offsets applied across a regular grid. A clear peak $(n_{\mathrm{x}} - \bar{n} = 90)$ is observed at the central point (zero offset), indicating a statistically significant positional correlation between the optical sources and the X-ray detections. This provides strong evidence that a subset of the X-ray sources is physically associated with optical counterparts in IC 10. A detailed interpretation is given in Section 6.

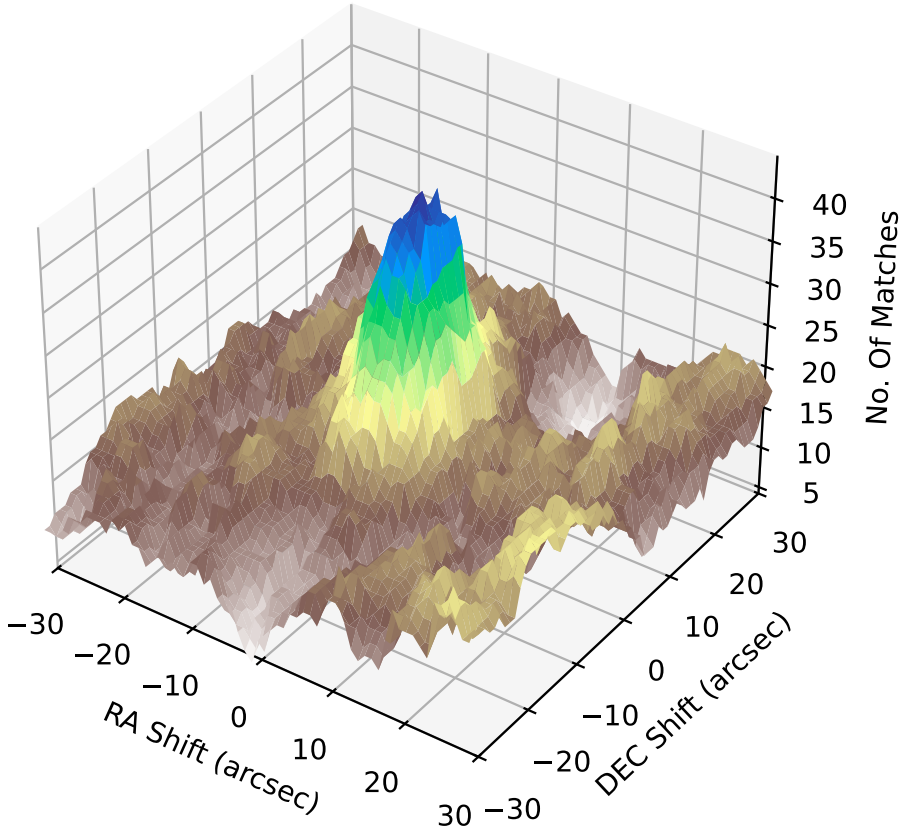

Figure 3. The peak-up test result for BSG candidate counterparts in IC 10. The plot shows the number of matches ($n_x - \bar{n}$) between X-ray and optical sources as a function of small coordinate offsets applied across a regular grid. A clear peak ($n_x - \bar{n} = 29$) is observed at the central point (zero offset), indicating a statistically significant positional correlation between the BSG optical sources and the X-ray detections. This provides strong evidence that a subset of the X-ray sources is physically associated with BSG counterparts in IC 10. A detailed interpretation is given in Section 6.

The peak-up test code used here utilizes *Starbase* for catalog matching purposes, whereas *Python* is used for data analysis and visualization (see Figures 2 and 3). In each iteration, if the number of matches (n_x) exceeds the median number expected by chance ($\bar{n}$), then a peak is observed in the two-dimensional mapping of the two catalogs, hence the name peak-up test. The significance of the peak is then calculated using the standard deviation (σ) of the distribution of chance alignments after removing the area within the maximum matching radius r_m of the zero-offset position. The significance S of the positional correlation peak is then expressed as

$$S = (n_x - \bar{n})/\sigma\,.$$

The matching of our final X-ray source catalog with the optical catalog by Massey et al. [19] resulted in the values of

$$n_x = 144, \quad \bar{n} = 54, \quad \sigma = 4.36, \quad \text{and} \quad S = 20.6 \quad (\text{XRB sources})\,.$$

Next, following the assessment of Massey et al. [19], who divided the color–magnitude space into foreground main sequence stars and IC 10 BSG stars, we also filtered the XRB catalog to match only BSG candidates obeying the criteria that $V > 19.5$ and $B - V < 1.5$. We thus obtained the values of

$$n_x = 44, \quad \bar{n} = 15, \quad \sigma = 2.69, \quad \text{and} \quad S = 10.8 \quad (\text{BSG candidates})\,.$$

The high significance values in both cases confirm that the positional correlation is not due to chance but rather due to the physical association of the pairs, thus reinforcing the expectation that many of the X-ray sources in IC 10 have massive stellar counterparts.

7. Discussion

IC 10 has been found to harbor a dense population of X-ray sources. The identification of individual X-ray sources in IC 10 is not an easy task due to its low galactic latitude position ($b = -3.3°$). Not only does the galactic H I column density interfere, but there is also interference from molecular gas in the galaxy and the gas inside IC 10 itself [15].

The presence of many more point sources, even though some of them are scattered around the edge of the galaxy, is one of the noteworthy additions made in this latest version of the IC 10 source catalog. Their spatial distribution offers important hints about the underlying stellar populations and the areas with higher star formation activity, although certain unrelated objects (AGN, SNRs, galactic sources) are bound to be superposed onto the IC 10 field.

7.1. Present Limitations and Future Work

The new catalog strives to present only XRB and BSG-XRB candidates, and filtering the list by color–magnitude may offer some assurance at least for BSG candidates. On the other hand, by utilizing the entire ACIS field of view for source detection, we unavoidably covered a region larger than the optical extent of IC 10. While this wide coverage enhances the completeness of the X-ray catalog, it also introduces certain X-ray sources not physically associated with IC 10. The actual IC 10 members will need to be confirmed by follow-up spectroscopic measurements of the Doppler shifts in nebular lines. Furthermore, the optical catalog in Ref. [19] has a limiting V magnitude of 23.8, which indicates that ∼50% of the optical counterparts are currently missing [21]. A deeper optical catalog will be able to assess the completeness of the current work.

7.2. Variable Sources

One of our main motivations was to look for variability in transient X-ray sources. IC 10 X-2 (Source 46) is a well-known transient (SFXT), whereas IC 10 X-1 (Source 20) is the brightest known persistent source in the galaxy. Laycock et al. [16] calculated the variability in the first 110 X-ray sources in our catalog and discussed some of them in detail. Here, we turn our attention to the new variable sources 246, 268, and 314 that have optical counterparts (although only 314 can be unambiguously classified as a BSG-HMXB):

- Source 246 (RA: 5.11538°; DEC: 59.1045°) is a persistent source (4/4 detections) with relative variability $\sigma = 5.49$. It has an optical counterpart in the catalog by Massey et al. [19] with $V = 18.215$ and $B - V = 1.71$. Its brightness and color information suggest that it is most likely a galactic source.
- Source 268 (RA: 5.19171°; DEC: 59.0732°) is a persistent source (3/3 detections) with relative variability $\sigma = 5.66$. It has an optical counterpart in the catalog by Massey et al. [19] with $V = 20.46$ and $B - V = 1.92$. Its brightness and color information suggest that it may be either a galactic source or an IC 10 yellow supergiant.
- Source 314 (RA: 5.30692°; DEC: 59.3676°) is a persistent source (5/5 detections) with relative variability $\sigma = 6.13$. It has an optical counterpart in the catalog by Massey et al. [19] with $V = 22.71$ and $B - V = 1.17$. Its brightness and color information suggest that it is a strong contender for an IC 10 BSG-HMXB source.

7.3. Characteristics of BSG-HMXB Systems

The BSG X-ray sources that we detected in our survey are accreting compact object binaries. BSGs can emit X-rays in isolation [25], as well as in compact object binaries, but at the distance of IC 10 (660 kpc), the observed X-ray fluxes can only be explained by accretion onto a compact object. The X-ray/optical (distance-independent) luminosity relationship was calculated for all sources with counterparts, viz.

$$\log(f_X/f_V) \;=\; \log(f_X) \;+\; V/2.5 \;+\; 5.37\,,$$

using the V magnitudes from the catalog by Massey et al. [19] and the measured X-ray fluxes (f_X) in the broad band (0.3–8 keV). Laycock et al. [21] showed that the BSG candidates have systematically higher f_X/f_V values, and the Mann–Whitney–Wilcoxon test showed statistically significant offsets between BSG candidates and other types of counterparts.

Known BSG sources have also shown significant X-ray variability in the 2010 *Chandra* monitoring data of IC 10. Variability ranges from a factor of ∼150 (for IC 10 X-2) to a factor of a few. Massey et al. [19] performed a narrow-band photometric survey to particularly identify luminous blue variable (LBV) candidates, but only IC 10 X-2 was found to be in that catalog. This might be because the selection criteria were based on M31. The authors showed that their filtering excluded 17 known WR stars in the field of IC 10. A new relaxed emission-line catalog can probably identify more LBV counterparts to the X-ray sources found in IC 10.

7.4. Population Estimates from the Census of BSG-XRB Candidates

The IC 10 BSG candidates can be used as a tracer to identify the underlying population of double-degenerate systems. If we assume that the $n_x = 44$ (from the peak-up test) BSG-XRB sources in IC 10 are all HMXBs, then their production rate and the number of precursor double-degenerate binaries can be estimated along the lines of Laycock et al. [21].

The duty cycle during which the LBVs are donating mass to their compact companions is $D = t_m/T$, where $T = 6$ Myr is the duration of the starburst in IC 10, and t_m is the mean lifetime of the LBVs, taken to be t_m = 0.4 Myr for a typical LBV mass of $30M_\odot$ [26–28]. For this duty cycle, IC 10 must have produced

$$n_{PDD} \;=\; n_x/D$$

precursor double-degenerate binaries during the course of the starburst.

From the above estimates, we determine typical values of $D = 1/15$ and $n_{PDD} = 660$ progenitors. This n_{PDD} value is nearly 3× larger than that previously determined by Laycock et al. [21] for IC 10. However, our estimate of double-degenerate progenitors was derived under simplified assumptions regarding the duty cycle and the LBV phase duration. It should therefore be regarded as a preliminary upper limit, which is subject to order-of-magnitude, model-dependent uncertainties dominated by systematic effects.

A comparison with gravitational-wave merger rates can be achieved by considering the fraction of HMXB progenitors that remain bound after both supernova explosions and common-envelope evolution, eventually forming merging compact binaries. Binary population synthesis studies (e.g., Ref. [29]) generally find that only a small fraction of massive interacting binaries (∼1–10%) successfully evolve into merging double-degenerate systems within a Hubble time. Thus, the application of these efficiencies to our inferred n_{PDD}∼660 progenitors results in about 7–66 merging compact binaries. Scaled to a volumetric rate by the star formation density of IC 10 (as in Ref. [21]), this yields a merger rate broadly consistent with the observed *LIGO/Virgo/KAGRA* constraints on BH–BH and BH–NS mergers (∼10–100 $\mathrm{Gpc^{-3}\,yr^{-1}}$). Although ours is only an order-of-magnitude

estimate, this comparison suggests that the BSG–HMXB pathway in IC 10 can contribute non-negligibly to the observed gravitational-wave population.

8. Summary and Conclusions

8.1. Summary

From the very first study by Wang et al. [15], it was evident that IC 10 hosts quite a few X-ray sources. Laycock et al. [16] followed up with an extensive study of the core region of IC 10 using *Chandra* monitoring data. In this work, we expanded both the field of view and the temporal baseline of the search by adding a recent 2021 observation and by analyzing data from all active CCDs during each observation.

We used `wavedetect` on soft, medium, hard, and broad-band images for source detection. A total of 375 X-ray point sources were detected in this search. The variability in these sources was classified using the individual observation source list. In the final comprehensive catalog, the *Chandra* and *XMM* source catalogs were also incorporated, and the first 110 sources from Laycock et al. [16] were kept intact to ensure a smooth extension of the original source catalog.

The new point source catalog was matched with the optical catalog by Massey et al. [19] to look for the X-ray binary population. We found 146 XRB sources with an optical counterpart down to the limiting V magnitude of 23.8. These XRB sources were subsequently filtered using the optical criteria $V > 19.5$ and $B - V < 1.5$ [19], resulting in 60 candidates of BSG optical companions.

8.2. Conclusions

We can already see that the new HMXBs reported here do not belong to the same HMXB population found in the Magellanic Clouds. The projected X-ray binary population of IC 10 is affected by the very young age of the underlying stellar population (∼6 Myr) and the enhanced formation of massive stars and stellar remnants reported by other authors [19,30]. The main differences concern the presence or absence of Be-HMXBs.

- SMC Be-HMXBs: At least 100 known or candidate HMXBs, the bulk of which are Be+NS systems and all of which have counterparts earlier than B3, are found in the SMC with its episodic starburst history [31]. Negueruela [32] originally suggested that the Be-HMXB restricted spectral type range is an evolutionary hallmark. The work of Antoniou et al. [13], which demonstrated that SMC Be-HMXBs are connected with separate populations of ages 40–70 Myr, lends weight to this theory. (In NGC 300 and NGC 2403, the next targets of opportunity, Williams et al. [33] discovered a comparable age association for HMXBs.) In a recent study using the modified BPASS model X-BPASS [34], it was shown that the X-ray population can contribute significantly to nebular He II emission. This catalog can provide important inputs regarding the number of X-ray sources and accretion rates (derived from X-ray luminosities) for modeling efforts regarding IC 10 and related systems.
- IC 10 BSG-XRBs and WR stars: Thus, we expected to see entirely different HMXB species in IC 10 because of the young age of its starburst. With the Be phenomenon not yet prevalent in IC 10, there should be other mass donors with stronger winds and/or lower orbital separations that provide the necessary mass transfer rates and accretion-powered X-ray emissions. The most obvious candidates are BSGs and WR stars, although only one X-ray source (IC 10 X-1; source 20 in Table 2) matches the WR catalog of Crowther et al. [35]. On the other hand, weak-lined WR stars may actually exist in IC 10, but they have not been recognized yet.

Author Contributions: Formal analysis, Investigation, and Methodology, S.B., S.G.T.L., B.A.B. and D.M.C.; Conceptualization and Project administration, S.G.T.L. and D.M.C.; Resources and Supervision, S.G.T.L. and B.A.B.; Writing—original draft, S.B.; Writing—review and editing, S.G.T.L., B.A.B. and D.M.C. All authors have read and agreed to the published version of the manuscript.

Funding: This research project was facilitated in part by the following funding agencies and programs: NSF-AAG, grant 2109004; NASA Astrophysics Data Analysis Program (ADAP), grants NNX14AF77G and 80NSSC18K0430; and the Lowell Center for Space Science and Technology (LoCSST) of the University of Massachusetts Lowell.

Data Availability Statement: The raw X-ray data can be downloaded from the *Chandra* data archive, URL: https://cxc.harvard.edu/cda/ (accessed on 15 August 2025). The full point source catalog and the long-term lightcurves of all detected X-ray sources are provided as supplements in Ref. [18] with URL: https://doi.org/10.7910/DVN/Y3PUOO (accessed on 10 September 2025).

Acknowledgments: We thank the reviewers of this paper for their constructive comments and suggestions that have led to improvements in its presentation. The support from NASA, NSF, and LoCSST over the years is gratefully acknowledged by the authors.

Conflicts of Interest: The authors declare no conflicts of interest.

Abbreviations

The following abbreviations are used in this manuscript:

ACIS	Advanced CCD Imaging Spectrometer
AGN	Active Galactic Nuclei
BCD	Blue Compact Dwarf
BH	Black Hole
BPASS	Binary Population And Spectral Synthesis
BSG	Blue Supergiant
CCD	Charge-Coupled Device
CIAO	Chandra Interactive Analysis of Observations
CSC	Chandra Source Catalog
DEC	DEClination
FOV	Field Of View
HMXB	High-Mass X-ray Binary
KAGRA	KAmioka GRAvitational-wave detector
LBV	Luminous Blue Variable
LIGO	Laser Interferometer Gravitational-wave Observatory
LMC	Large Magellanic Cloud
NS	Neutron Star
PSF	Point Spread Function
RA	Right Ascension
SFXT	Supergiant Fast X-ray Transient
SG	Supergiant
SMC	Small Magellanic Cloud
SNR	Supernova Remnant
WR	Wolf–Rayet
XRB	X-ray Binary

Appendix A

The XRB and BSG-XRB candidates in the IC 10 field are listed in Tables A1–A4 and Tables A5 and A6, respectively. Some sources have unknown or unphysical $B - V$ values, and such entries are marked by dashes. All sources are identified by their X-ray catalog ID ('Source #'), but multiple optical counterparts may exist within the matching radius; such

cases have multiple entries, but the optical counterpart properties (color and magnitude) are different. Multiple entries are marked by arrows in the 'Source #' columns of the tables.

Additionally, the full point source catalog and the long-term lightcurves of all detected X-ray sources can be downloaded from the link https://doi.org/10.7910/DVN/Y3PUOO (see also Ref. [18]).

Table A1. IC 10 X-ray binary candidates (among numbered sources 1–100).

Source #	RA	DEC	V_{mag}	$B-V$
1	5.03621	59.2279	22.384	0.7
3	5.06636	59.2399	20.247	1.57
4	5.02508	59.2402	22.588	1.92
7	5.11086	59.2487	16.985	1.497
8	5.05286	59.2504	22.974	1.242
13	4.99465	59.2576	20.473	1.525
15	5.03663	59.2624	16.758	1.174
17	5.14415	59.2659	16.381	1.186
→ 17	5.14415	59.2659	16.372	1.196
20 (X-1)	5.12132	59.281	22.478	0.017
→ 20 (X-1)	5.12132	59.281	21.722	0.905
21	5.03429	59.2818	23.486	1.878
25	5.10117	59.2892	22.856	0.82
→ 25	5.10117	59.2892	22.441	0.77
26	4.97811	59.2894	21.983	1.338
→ 26	4.97811	59.2894	22.04	1.271
27	5.04657	59.2908	21.924	0.844
28	5.19383	59.292	18.793	1.521
29	5.0382	59.2939	21.777	1.059
→ 29	5.0382	59.2939	21.732	0.932
32	5.04812	59.304	20.428	1.54
38	5.03305	59.3124	22.344	1.85
39	5.10836	59.3125	18.878	1.64
46 (X-2)	5.08723	59.2997	19.954	1.211
48	5.17812	59.3144	17.954	1.441
50	5.19656	59.3267	22.539	1.823
52	5.1391	59.3596	17.277	1.551
53	5.05732	59.3766	21.404	1.872
61	5.13621	59.2626	21.296	1.877
65	5.08036	59.3043	23.685	0.789
→ 65	5.08036	59.3043	23.737	1.043
66	4.92791	59.3347	17.625	1.103
→ 66	4.92791	59.3347	17.6	1.133
76	5.1187	59.3358	17.382	1.125
77	5.0722	59.2972	23.059	1.734
78	5.09598	59.2982	21.411	0.705
→ 78	5.09598	59.2982	22.152	0.581
→ 78	5.09598	59.2982	22.445	0.786
86	5.15428	59.3134	18.727	1.295
87	5.03887	59.3919	18.75	1.304
90	5.11847	59.3399	21.348	1.805
91	4.9653	59.2619	20.749	1.533
92	4.99881	59.3009	21.471	0.725
96	5.05331	59.2723	22.038	1.325
98	5.0508	59.2844	23.142	2.046
→ 98	5.0508	59.2844	22.101	1.874
→ 98	5.0508	59.2844	22.315	0.623
→ 98	5.0508	59.2844	23.155	0.587
100	5.01024	59.3015	23.097	0.708

Table A2. IC 10 X-ray binary candidates (among numbered sources 101–200).

Source #	RA	DEC	V_{mag}	$B-V$
101	5.11942	59.3493	20.697	1.646
106	5.04294	59.317	21.99	2.263
107	5.20919	59.2572	20.083	1.743
133	4.79151	59.2074	20.865	1.909
139	4.82537	59.2088	16.256	0.98
140	4.82668	59.2352	22.87	–
143	4.83621	59.211	18.809	1.189
144	4.84389	59.2613	21.624	1.697
145	4.85256	59.3573	19.141	−0.102
→ 145	4.85256	59.3573	17.631	1.672
→ 145	4.85256	59.3573	17.802	1.471
147	4.85651	59.2385	18.134	1.616
148	4.85799	59.1303	21.139	1.104
→ 148	4.85799	59.1303	23.675	1.044
150	4.86137	59.1846	16.674	1.147
151	4.86395	59.2373	18.829	1.624
153	4.86454	59.408	23.702	2.031
157	4.88205	59.2357	23.677	1.175
167	4.91239	59.3839	16.602	1.055
168	4.91505	59.1706	23.198	0.899
169	4.91716	59.462	18.189	1.371
173	4.92518	59.0735	21.55	2.071
176	4.93644	59.2304	16.131	0.634
→ 176	4.93644	59.2304	20.183	–
179	4.94619	59.2133	15.961	1.054
180	4.95156	59.332	22.701	1.456
181	4.95463	59.106	22.867	0.937
182	4.95562	59.2261	18.252	1.405
183	4.96093	59.3249	21.865	−0.183
→ 183	4.96093	59.3249	20.888	0.965
→ 183	4.96093	59.3249	20.38	1.562
184	4.96149	59.0785	23.496	0.81
186	4.96547	59.1423	20.475	1.029
188	4.96792	59.1179	22.302	1.867
197	4.98966	59.2978	22.832	1.659
198	4.99304	59.141	16.445	1.157
199	4.99389	59.12	22.638	1.488

Table A3. IC 10 X-ray binary candidates (among numbered sources 201–300).

Source #	RA	DEC	V_{mag}	$B-V$
201	4.99573	59.1517	22.065	1.71
→ 201	4.99573	59.1517	19.079	1.012
205	5.0055	59.373	22.526	1.193
213	5.0181	59.3976	23.163	1.704
214	5.01921	59.3124	21.204	1.572
216	5.03054	59.3257	22.878	0.807
217	5.03137	59.2137	22.361	1.299
222	5.05005	59.3885	19.262	1.514
223	5.05384	59.4846	22.489	0.98
227	5.06583	59.3197	19.593	1.278
228	5.06588	59.5057	23.303	1.108

Table A3. *Cont.*

Source #	RA	DEC	V_{mag}	$B-V$
230	5.07889	59.1956	20.225	1.724
232	5.07959	59.0874	22.996	1.639
233	5.0877	59.1783	17.71	0.953
234	5.0927	59.3465	19.382	1.557
237	5.09626	59.1371	22.238	1.216
238	5.0978	59.3075	22.467	0.606
→ 238	5.0978	59.3075	24.119	0.018
→ 238	5.0978	59.3075	23.392	0.635
241	5.10252	59.2938	21.782	0.677
→ 241	5.10252	59.2938	21.859	0.107
→ 241	5.10252	59.2938	23.46	1.334
→ 241	5.10252	59.2938	22.538	0.35
242	5.10649	59.2974	24.59	0.662
244	5.10888	59.3125	18.878	1.64
246	5.11538	59.1045	18.215	1.706
250	5.12773	59.3248	20.869	1.757
252	5.1407	59.1761	16.093	1.582
254	5.14407	59.1872	20.1	1.796
261	5.16485	59.2477	21.84	1.903
262	5.16504	59.2369	20.243	1.735
265	5.18	59.1264	23.491	0.984
267	5.19123	59.2721	20.178	1.719
268	5.19171	59.0732	20.56	1.921
272	5.19677	59.2228	17.733	1.488
275	5.20739	59.2083	20.898	1.8
281	5.22531	59.427	18.018	1.64
293	5.24541	59.3558	17.839	1.393
295	5.24921	59.2232	23.7	0.662
296	5.25044	59.1017	23.339	2.043
300	5.26496	59.3152	19.258	1.024
→ 300	5.26496	59.3152	23.238	1.854

Table A4. IC 10 X-ray binary candidates (among numbered sources 301–375).

Source #	RA	DEC	V_{mag}	$B-V$
301	5.26571	59.3451	22.54	1.387
303	5.26806	59.107	18.514	1.579
307	5.28589	59.141	18.531	1.343
308	5.28685	59.1925	23.139	1.158
314	5.30692	59.3676	22.706	1.17
316	5.31863	59.3442	22.232	1.702
318	5.32064	59.373	19.224	1.456
323	5.3277	59.4037	22.069	1.856
324	5.33041	59.4016	20.119	1.202
326	5.33145	59.0841	20.851	1.65
331	5.3445	59.3494	23.267	0.928
333	5.35647	59.3179	18.943	1.725
335	5.36187	59.4023	22.821	1.972
343	5.38665	59.2442	21.469	0.875
346	5.40615	59.3394	22.994	0.987
348	5.41238	59.3784	18.817	1.672

Table A5. IC 10 blue supergiant X-ray binary candidates (among numbered sources 1–200).

Source #	RA	DEC	V_{mag}	$B-V$
1	5.03621	59.2279	22.384	0.7
8	5.05286	59.2504	22.974	1.242
20 (X-1)	5.12132	59.281	22.478	0.017
→ 20 (X-1)	5.12132	59.281	21.722	0.905
25	5.10117	59.2892	22.441	0.77
→ 25	5.10117	59.2892	22.856	0.82
26	4.97811	59.2894	21.983	1.338
→ 26	4.97811	59.2894	22.04	1.271
27	5.04657	59.2908	21.924	0.844
29	5.0382	59.2939	21.777	1.059
→ 29	5.0382	59.2939	21.732	0.932
46 (X-2)	5.08723	59.2997	19.954	1.211
65	5.08036	59.3043	23.737	1.043
→ 65	5.08036	59.3043	23.685	0.789
78	5.09598	59.2982	21.411	0.705
→ 78	5.09598	59.2982	22.152	0.581
→ 78	5.09598	59.2982	22.445	0.786
92	4.99881	59.3009	21.471	0.725
96	5.05331	59.2723	22.038	1.325
98	5.0508	59.2844	22.315	0.623
→ 98	5.0508	59.2844	23.155	0.587
100	5.01024	59.3015	23.097	0.708
145	4.85256	59.3573	19.141	−0.102
148	4.85799	59.1303	21.139	1.104
→ 148	4.85799	59.1303	23.675	1.044
157	4.88205	59.2357	23.677	1.175
168	4.91505	59.1706	23.198	0.899
176	4.93644	59.2304	20.183	–
180	4.95156	59.332	22.701	1.456
181	4.95463	59.106	22.867	0.937
183	4.96093	59.3249	21.865	−0.183
→ 183	4.96093	59.3249	20.888	0.965
184	4.96149	59.0785	23.496	0.81
186	4.96547	59.1423	20.475	1.029
199	4.99389	59.12	22.638	1.488

Table A6. IC 10 blue supergiant X-ray binary candidates (among numbered sources 201–375).

Source #	RA	DEC	V_{mag}	$B-V$
201	4.99573	59.1517	19.079	1.012
205	5.0055	59.373	22.526	1.193
216	5.03054	59.3257	22.878	0.807
217	5.03137	59.2137	22.361	1.299
223	5.05384	59.4846	22.489	0.98
227	5.06583	59.3197	19.593	1.278
228	5.06588	59.5057	23.303	1.108
237	5.09626	59.1371	22.238	1.216
238	5.0978	59.3075	23.392	0.635
→ 238	5.0978	59.3075	24.119	0.018
→ 238	5.0978	59.3075	22.467	0.606
241	5.10252	59.2938	21.782	0.677

Table A6. *Cont.*

Source #	RA	DEC	V_{mag}	$B-V$
→ 241	5.10252	59.2938	21.859	0.107
→ 241	5.10252	59.2938	23.46	1.334
→ 241	5.10252	59.2938	22.538	0.35
242	5.10649	59.2974	24.59	0.662
265	5.18	59.1264	23.491	0.984
295	5.24921	59.2232	23.7	0.662
300	5.26496	59.3152	19.258	1.024
301	5.26571	59.3451	22.54	1.387
308	5.28685	59.1925	23.139	1.158
314	5.30692	59.3676	22.706	1.17
318	5.32064	59.373	19.224	1.456
324	5.33041	59.4016	20.119	1.202
331	5.3445	59.3494	23.267	0.928
343	5.38665	59.2442	21.469	0.875
346	5.40615	59.3394	22.994	0.987

References

1. Mayall, N. An extra-galactic object 3 from the plane of the galaxy. *Publ. Astron. Soc. Pac.* **1935**, *47*, 317. [CrossRef]
2. Hubble, E. The luminosity function of nebulae. I. The luminosity function of resolved nebulae as indicated by their brightest stars. *Astrophys. J.* **1936**, *84*, 158. [CrossRef]
3. Gonçalves, D.R.; Teodorescu, A.M.; Alves-Brito, A.; Méndez, R.H.; Magrini, L. A kinematic study of planetary nebulae in the dwarf irregular galaxy IC10. *Mon. Not. R. Astron. Soc.* **2012**, *425*, 2557–2566. [CrossRef]
4. Sanna, N.; Bono, G.; Stetson, P.; Monelli, M.; Pietrinferni, A.; Drozdovsky, I.; Caputo, F.; Cassisi, S.; Gennaro, M.; Moroni, P.P.; et al. On the distance and reddening of the starburst galaxy IC 10. *Astrophys. J.* **2008**, *688*, L69. [CrossRef]
5. Massey, P.; Armandroff, T.E.; Conti, P.S. IC 10-A "poor cousin" rich in Wolf-Rayet stars. *Astron. J.* **1992**, *103*, 1159–1165, 1421. [CrossRef]
6. Massey, P.; Armandroff, T.E. The Massive Star Content, Reddening, and Distance of the Nearby Irregular Galaxy IC 10. *Astron. J.* **1995**, *109*, 2470. [CrossRef]
7. Hodge, P.; Lee, M.G. The H II regions of IC 10. *Publ. Astron. Soc. Pac.* **1990**, *102*, 26. [CrossRef]
8. Hunter, D.A.; Gallagher, J.S. Star-forming properties and histories of dwarf irregular galaxies-Down but not out. *Astrophys. J. Suppl. Ser.* **1985**, *58*, 533–560; ISSN 0067-0049. [CrossRef]
9. Massey, P.; Armandroff, T.E.; Pyke, R.; Patel, K.; Wilson, C.D. Hot, luminous stars in selected regions of NGC 6822, M31, and M33. *Astron. J.* **1995**, *110*, 2715. [CrossRef]
10. Wilcots, E.M.; Miller, B.W. The kinematics and distribution of HI in IC 10. *Astron. J.* **1998**, *116*, 2363. [CrossRef]
11. Richer, M.; Bullejos, A.; Borissova, J.; McCall, M.L.; Lee, H.; Kurtev, R.; Georgiev, L.; Kingsburgh, R.; Ross, R.; Rosado, M. IC 10: More evidence that it is a blue compact dwarf. *Astron. Astrophys.* **2001**, *370*, 34–42. [CrossRef]
12. Nidever, D.L.; Ashley, T.; Slater, C.T.; Ott, J.; Johnson, M.; Bell, E.F.; Stanimirović, S.; Putman, M.; Majewski, S.R.; Simpson, C.E.; et al. Evidence for an interaction in the nearest starbursting dwarf irregular galaxy IC 10. *Astrophys. J. Lett.* **2013**, *779*, L15. [CrossRef]
13. Antoniou, V.; Zezas, A.; Hatzidimitriou, D.; Kalogera, V. Star formation history and X-ray binary populations: The case of the Small Magellanic Cloud. *Astrophys. J. Lett.* **2010**, *716*, L140. [CrossRef]
14. Binder, B.A.; Lazarus, R.; Thoresen, M.; Laycock, S.; Bhattacharya, S. The X-ray Variability and Luminosity Function of High Mass X-ray Binaries in the Dwarf Starburst Galaxy IC 10. *arXiv* **2025**, arXiv:2508.02876. [CrossRef]
15. Wang, Q.D.; Whitaker, K.E.; Williams, R. An XMM-Newton and Chandra study of the starburst galaxy IC 10. *Mon. Not. R. Astron. Soc.* **2005**, *362*, 1065–1077. [CrossRef]
16. Laycock, S.; Cappallo, R.; Williams, B.F.; Prestwich, A.; Binder, B.; Christodoulou, D.M. The X-ray Binary Population of the Nearby Dwarf Starburst Galaxy IC 10: Variable and Transient X-ray Sources. *Astrophys. J.* **2017**, *836*, 50. [CrossRef]
17. Hong, J.; van den Berg, M.; Schlegel, E.M.; Grindlay, J.E.; Koenig, X.; Laycock, S.; Zhao, P. X-ray processing of champlane fields: Methods and initial results for selected anti-galactic center fields. *Astrophys. J.* **2005**, *635*, 907. [CrossRef]
18. Bhattacharya, S. *Replication Data for: Chandra Observations of the X-Ray Binary Population in IC 10*; Harvard Dataverse: Cambridge, MA, USA, 2025. [CrossRef]

19. Massey, P.; McNeill, R.T.; Olsen, K.; Hodge, P.W.; Blaha, C.; Jacoby, G.H.; Smith, R.; Strong, S.B. A survey of local group galaxies currently forming stars. III. A search for luminous blue variables and other Hα emission-line stars. *Astron. J.* **2007**, *134*, 2474. [CrossRef]
20. Laycock, S.; Cappallo, R.; Oram, K.; Balchunas, A. A transient supergiant X-ray binary in IC 10: An extragalactic SFXT? *Astrophys. J.* **2014**, *789*, 64. [CrossRef]
21. Laycock, S.G.; Christodoulou, D.M.; Williams, B.F.; Binder, B.; Prestwich, A. Blue Supergiant X-ray Binaries in the Nearby Dwarf Galaxy IC 10. *Astrophys. J.* **2017**, *836*, 51. [CrossRef]
22. Pineau, F.X.; Derriere, S.; Motch, C.; Carrera, F.J.; Genova, F.; Michel, L.; Mingo, B.; Mints, A.; Gómez-Morán, A.N.; Rosen, S.R.; et al. Probabilistic multi-catalogue positional cross-match. *A&A* **2017**, *597*, A89.
23. Nguyen, T.; Basu, A.; Budavári, T. Globally optimal and scalable N-way matching of astronomy catalogs. *Astron. J.* **2022**, *163*, 296. [CrossRef]
24. Avdeeva, A.S.; Karpov, S.V.; Malkov, O.Y.; Zhao, G. Cross-Matching of Large Sky Surveys and Study of Astronomical Objects Apparent in Ultraviolet Band Only. In Proceedings of the International Conference on Data Analytics and Management in Data Intensive Domains, Moscow, Russia, 26–29 October 2021; Springer International Publishing: Cham, Switzerland, 2021; pp. 53–73.
25. Berghöfer, T.; Schmitt, J.; Danner, R.; Cassinelli, J. X-ray properties of bright OB-type stars detected in the ROSAT all-sky survey. *Astron. Astrophys.* **1997**, *322*, 167–174.
26. Maeder, A.; Meynet, G. Stellar evolution with rotation. VII.—Low metallicity models and the blue to red supergiant ratio in the SMC. *Astron. Astrophys.* **2001**, *373*, 555–571. [CrossRef]
27. Fragos, T.; Linden, T.; Kalogera, V.; Sklias, P. On the formation of ultraluminous x-ray sources with neutron star accretors: The case of m82 x-2. *Astrophys. J. Lett.* **2015**, *802*, L5. [CrossRef]
28. Massey, P.; Neugent, K.F.; Smart, B.M. A spectroscopic survey of massive stars in M31 and M33. *Astron. J.* **2016**, *152*, 62. [CrossRef]
29. Broekgaarden, F.S.; Berger, E.; Stevenson, S.; Justham, S.; Mandel, I.; Chruślińska, M.; van Son, L.A.C.; Wagg, T.; Vigna-Gómez, A.; de Mink, S.E.; et al. Impact of massive binary star and cosmic evolution on gravitational wave observations–II. Double compact object rates and properties. *Mon. Not. R. Astron. Soc.* **2022**, *516*, 5737. [CrossRef]
30. Bauer, F.E.; Brandt, W.N. Chandra and Hubble space telescope confirmation of the luminous and variable X-ray source ic 10 X-1 as a possible Wolf-Rayet, black hole binary. *Astrophys. J.* **2004**, *601*, L67. [CrossRef]
31. McBride, V.; Coe, M.; Negueruela, I.; Schurch, M.; McGowan, K. Spectral distribution of Be/X-ray binaries in the Small Magellanic Cloud. *Mon. Not. R. Astron. Soc.* **2008**, *388*, 1198–1204. [CrossRef]
32. Negueruela, I. On the nature of Be/X-ray binaries. *Astron. Astrophys.* **1998**, *338*, 505.
33. Williams, B.F.; Dalcanton, J.J.; Stilp, A.; Dolphin, A.; Skillman, E.D.; Radburn-Smith, D. The ACS nearby galaxy survey treasury. XI. The remarkably undisturbed NGC 2403 disk. *Astrophys. J.* **2013**, *765*, 120. [CrossRef]
34. Bray, J.C.; Stanway, E.R.; Eldridge, J.J. X-BPASS: Self-consistent modelling of stellar populations and their associated X-ray binary emission in a binary stellar evolution framework. *Mon. Not. R. Astron. Soc.* **2025**, *542*, 2087. [CrossRef]
35. Crowther, P.A.; Drissen, L.; Abbott, J.B.; Royer, P.; Smartt, S.J. Gemini observations of Wolf-Rayet stars in the Local Group starburst galaxy IC 10. *Astron. Astrophys.* **2003**, *404*, 483–493. [CrossRef]